

Supporting Information

Graphene-Based Cellular Materials with Extremely Low Density and High Pressure Sensitivity Based on Self-Assembled Graphene Oxide Liquid Crystals

Xianzhang Wu^{a,b}, Xiaohong Liu^a, Jingxia Huang^{a,b}, Jinqing Wang^{a,*}, and Shengrong Yang^a

*^a State Key Laboratory of Solid Lubrication, Lanzhou Institute of Chemical Physics,
Chinese Academy of Sciences, Lanzhou, 730000, P. R. China*

^b University of Chinese Academy of Sciences, Beijing, 100080, P. R. China

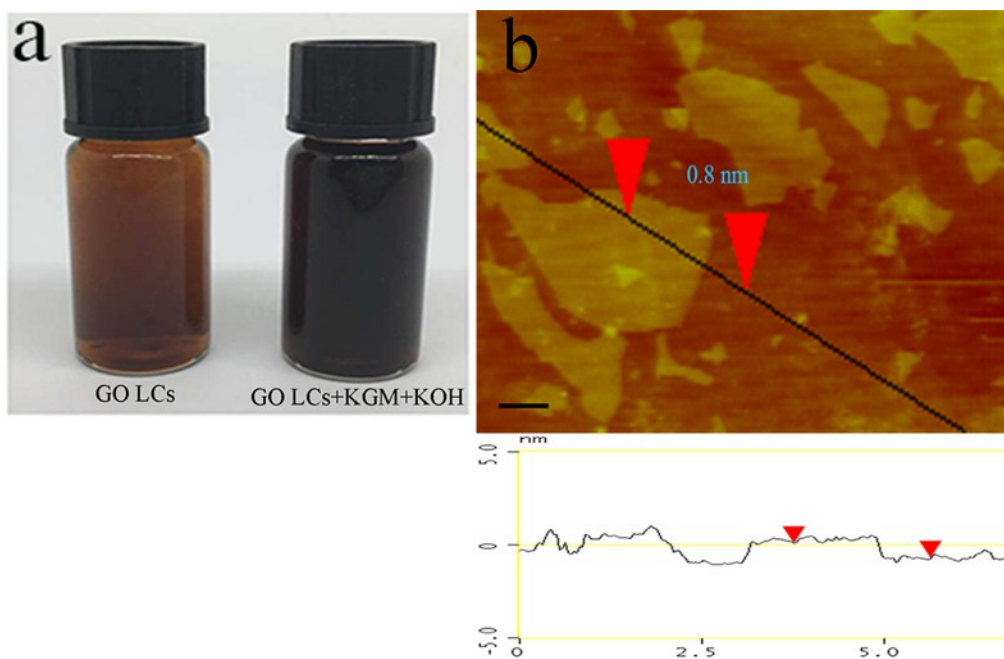


Fig. S1 (a) The photographs of 5 mL GO LCs suspension with a concentration of 1.7 mg mL^{-1} (left) and GO LCs + KGM + KOH suspension (right). (b) AFM image of GO nanosheets; Scale bar = $1 \mu\text{m}$.

The average lateral size of the GO LC nanosheet is measured as $3.5 \pm 1.8 \mu\text{m}$ with a thickness of about 0.8 nm, indicating it can be stably dispersed in water with single-layer structure.

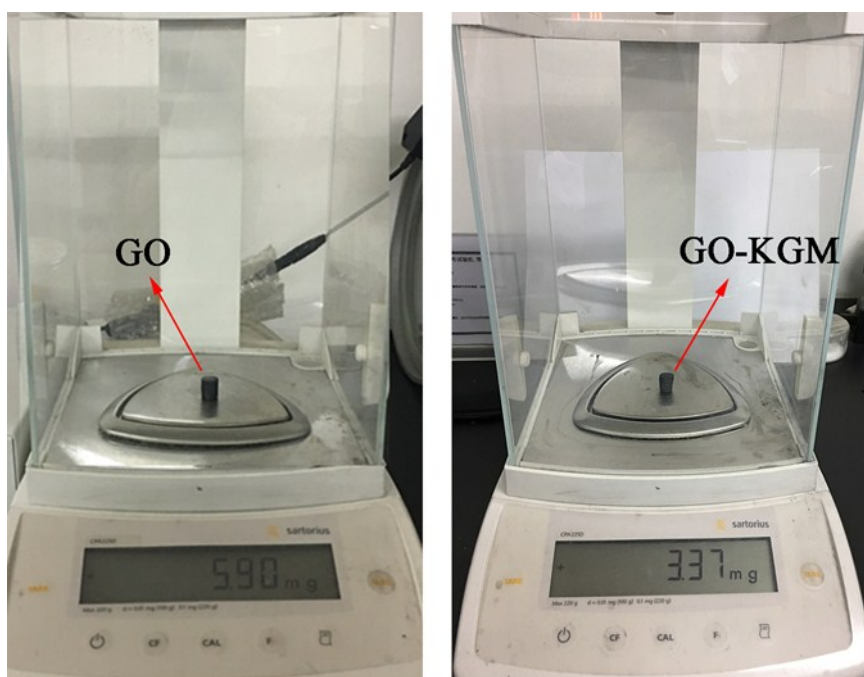


Fig. S2 The weight measurement processes for the GO with a density of 1.43 mg cm^{-3} (5.90 mg in 4.13 cm^{-3}) and for the GO-KGM with a density of 0.94 mg cm^{-3} (3.37 mg in 3.58 cm^{-3}).

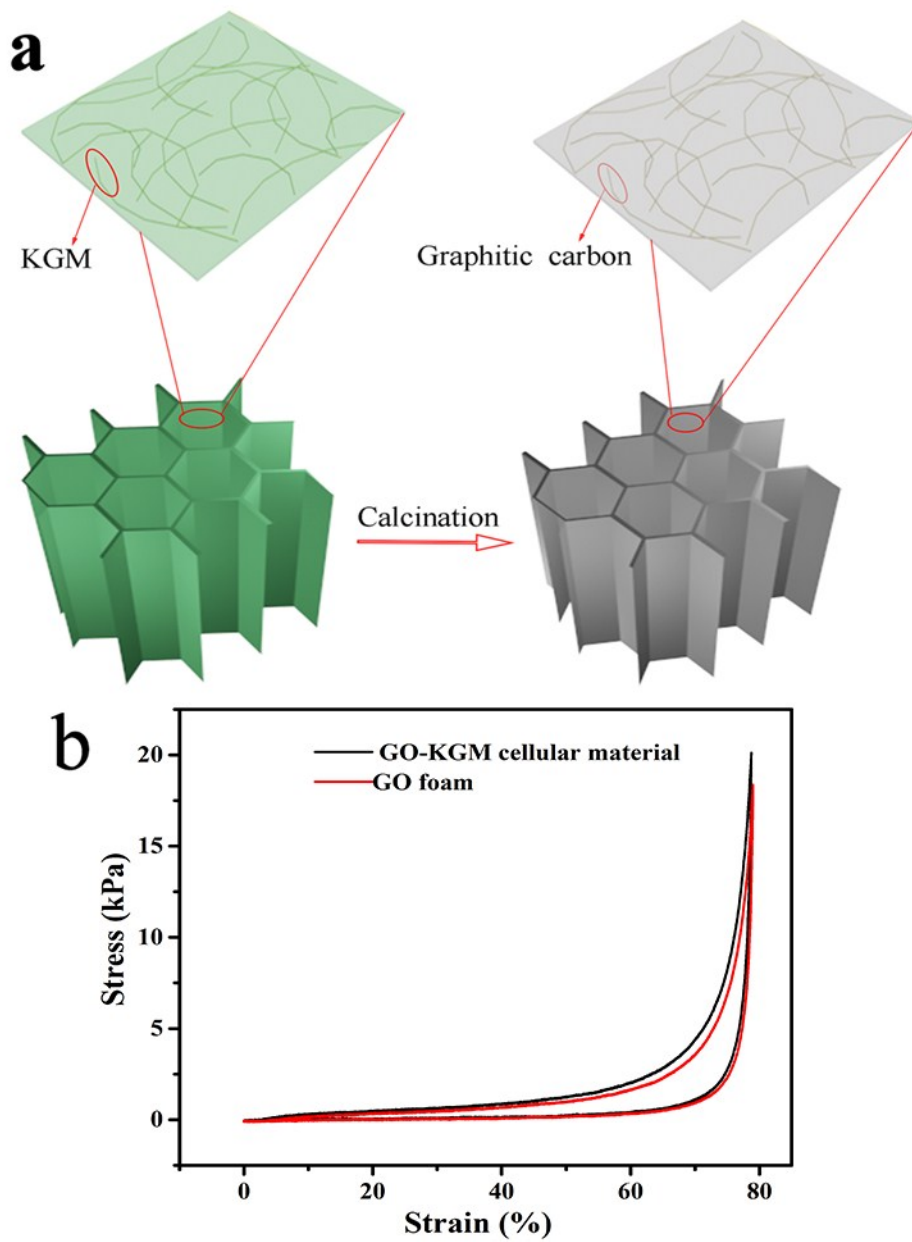


Fig. S3 (a) Cartoon models corresponding to the calcining process of GO-KGM. (b)

Compressive σ - ϵ curves of GO and GO-KGM.

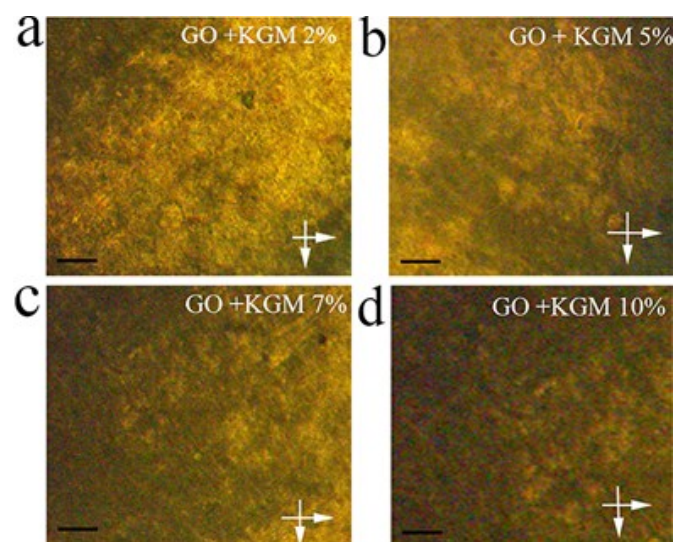


Fig. S4 POM images of GO + KGM suspensions with various KGM contents of (a) 2 wt%, (b) 5 wt%, (c) 7 wt%, and (d) 10 wt%; Scale bar: 300 μm .

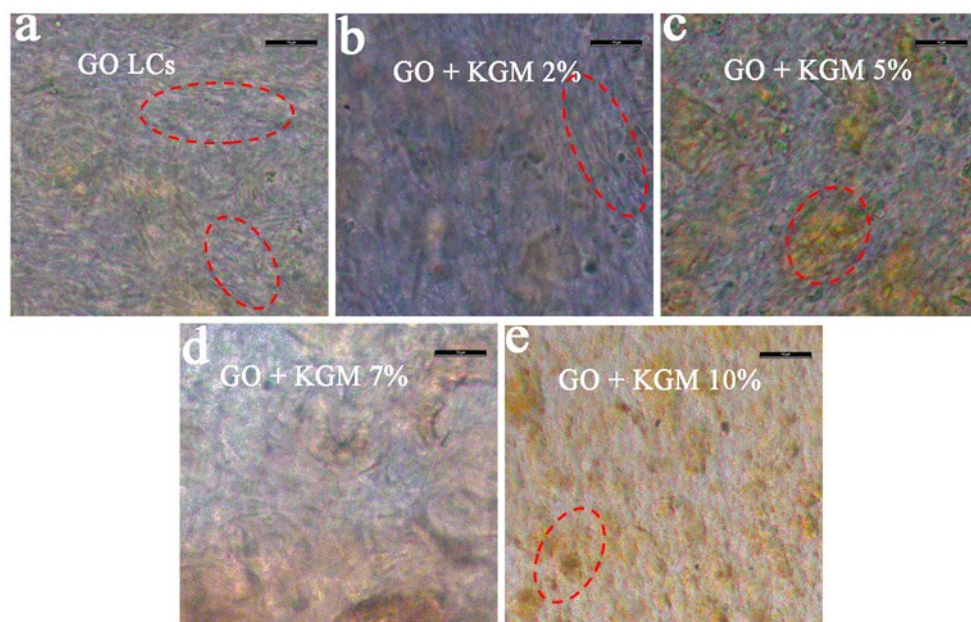


Fig. S5 Optical images of GO + KGM suspensions with different KGM contents of (a) 2 wt%, (b) 5 wt%, (c) 7 wt%, and (d) 10 wt%. Scale bar: 10 μm .

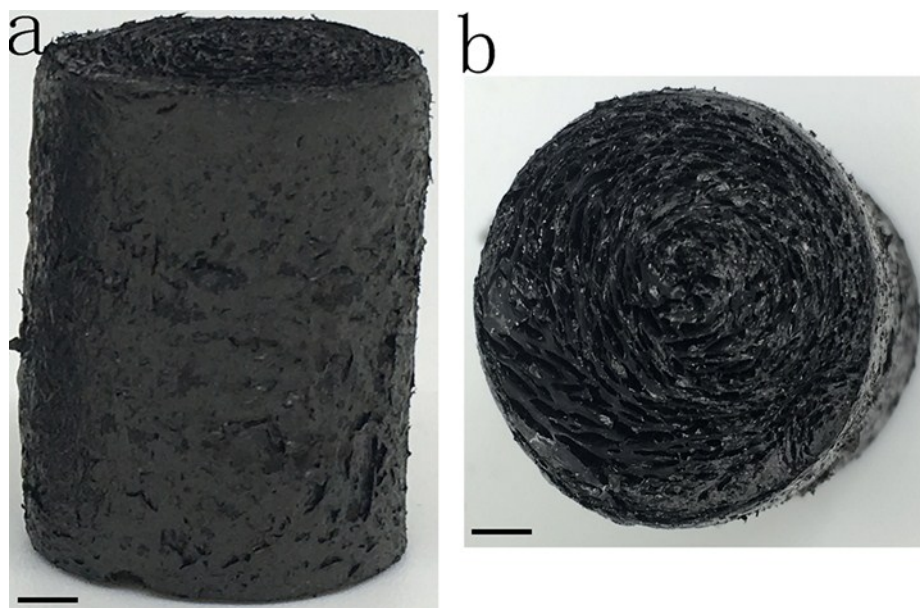


Fig. S6 The photographs of GO-KGM with different perspectives. (a) Front outline and (b) vertical views. GO-KGM shows a long-range ordered structure on the macro scale; Scale bar: 4 mm.

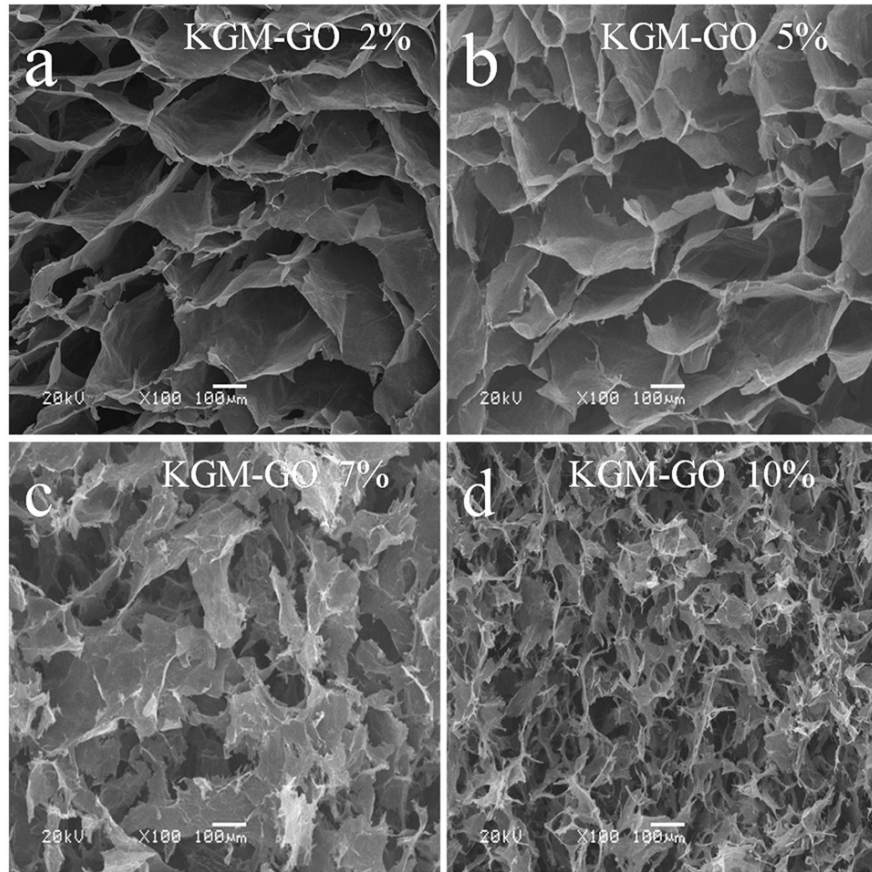


Fig.S7 SEM images of the GO-KGM cellular materials with different KGM contents of (a) 2 wt%, (b) 5 wt%, (c) 7 wt%, and (d) 10 wt%.

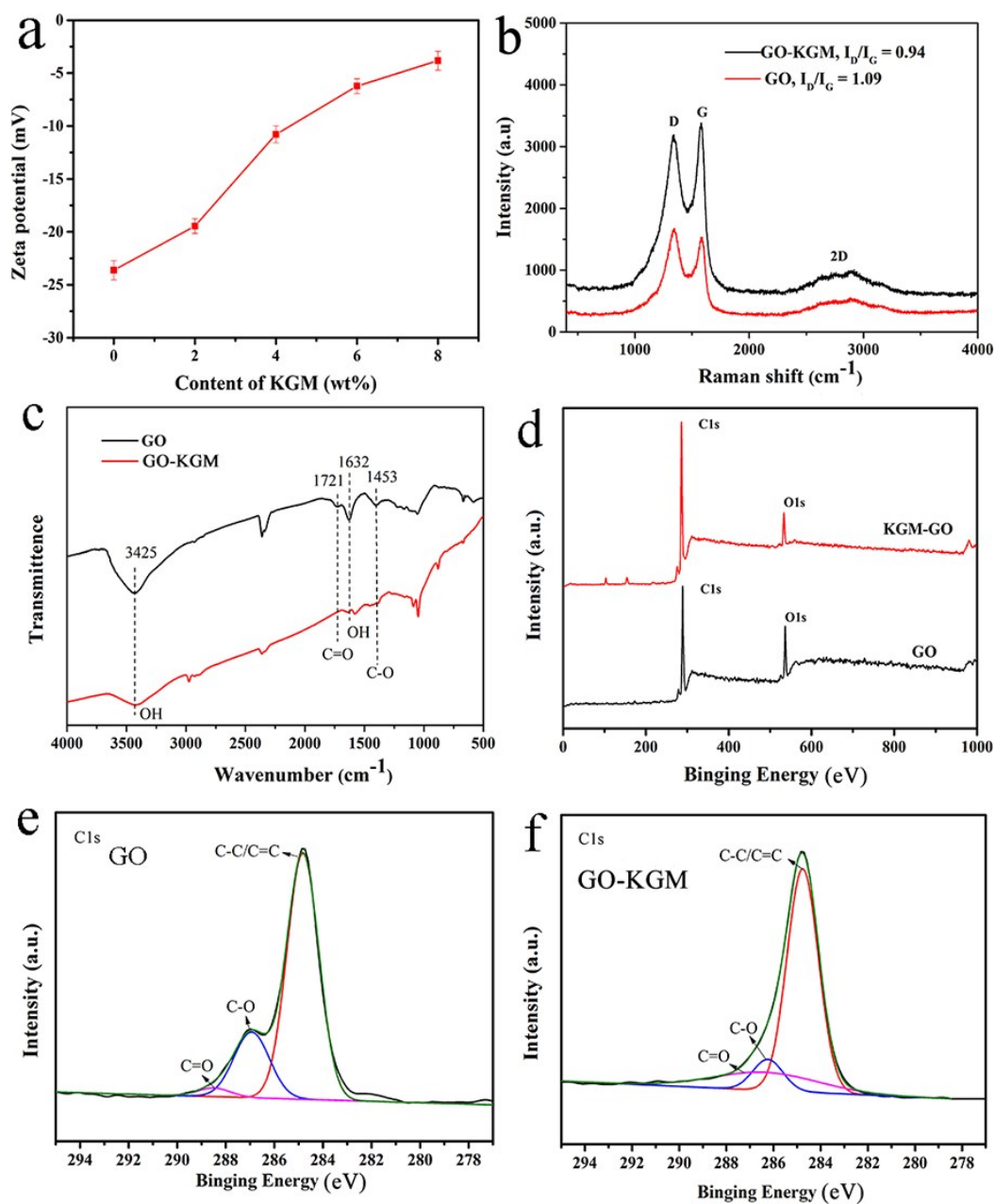


Fig. S8 Structural and chemical composition characterizations of samples. (a) The dependence of the zeta potential of GO + KGM suspensions on the contents of KGM. (b) Raman, (c) FT-IR and (d) XPS survey spectra of GO- KGM and GO. XPS C1s spectra of (e) GO and (f) GO-KGM.

The Raman spectra of GO and GO-KGM samples (Fig. S8b) show the typical D and G bands around 1340 and 1579 cm^{-1} .¹ The intensity ratios of I_D/I_G reduce from 1.09 for GO to 0.94 for GO-KGM, indicating that the oxygen functional groups have

been removed from the GO LCs sheets after the hydrothermal reduction and thermal treatment processes, resulting in the defects decrease on both sides of GO LCs sheets. The FT-IR spectra of GO and GO-KGM network provide further evidence that the GO-KGM is reduced after thermal treatment (Fig. S8c). Compared with GO foam, the obvious intensity decrease in the peaks at 3425 and 1632 cm^{-1} can be ascribed to vibrations and bending vibrations of residual O-H of the GO sheets. Meanwhile, the bands at 1721 and 1577 cm^{-1} are assigned to the bending vibrations of C=O and C-O,² whose intensities also decrease after thermal treatment. To further investigate the change of oxygen content at the treating temperature of 850 °C, X-ray photoelectron spectroscopy (XPS) analyses are conducted for both the GO and GO-KGM. As shown in Fig. S8d, the O1s peak intensity significantly decreases for GO-KGM while the C/O atomic ratio has increased to 11.2 compared to 4.8 for the GO foam. Fig.S8e,f show the C1s spectra, which can be curve-fitted into four peak components, corresponding to C=C double bond (284.8 eV), C-O single bonds (286.9 eV), and C=O double bond (288.0 eV), respectively.^{3,4} Comparing the spectra, the peaks intensities associating with oxygen- containing components of GO-KGM are significantly decrease, and C-C becomes dominant in GO-KGM. This implies that the GO-KGM is effectively deoxidized during hydrothermal reduction and subsequent thermal annealing steps, which is well accordance with the Raman and FT-IR results in Fig.S8b, c.

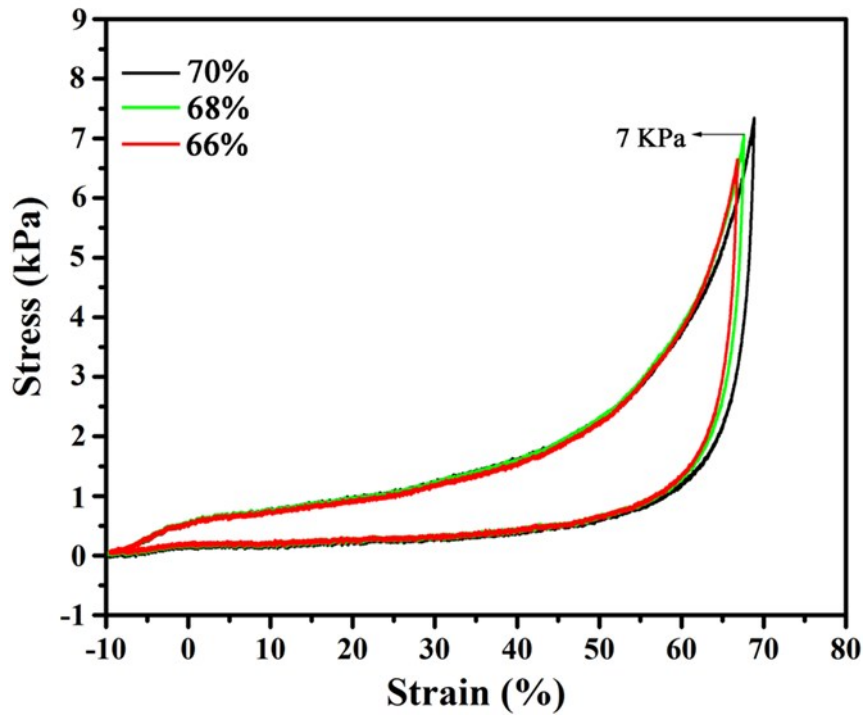


Fig. S9 The stress-strain curves of GO-KGM at set strains of 66%, 68%, 70% and 80%, respectively.

As shown in Fig. S9 that at maximal deformation of 66% and 68% the stress-strain curves are reproduced on the next cycle. Once the maximum deformation is increased to 70%, the “forward branch” of the stress-strain curve begins to fall below this branch of the previous cycle. Because the strain is too small to be further refined, therefore, we think the critical value of the stress is 7kPa.

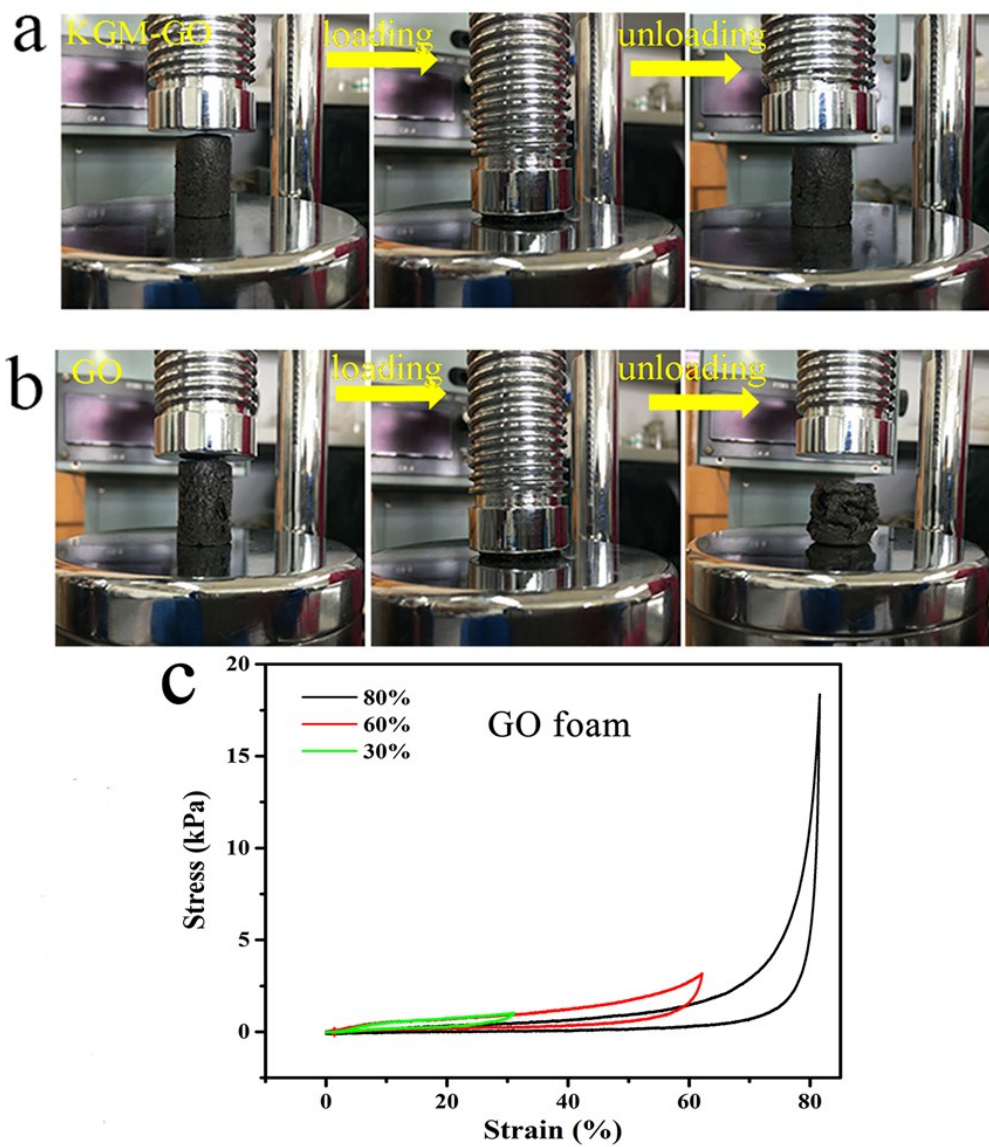


Fig. S10 The photographs of the compression performance for (a) GO-KGM and (b) GO. (c) Compressive σ - ε curves of GO.

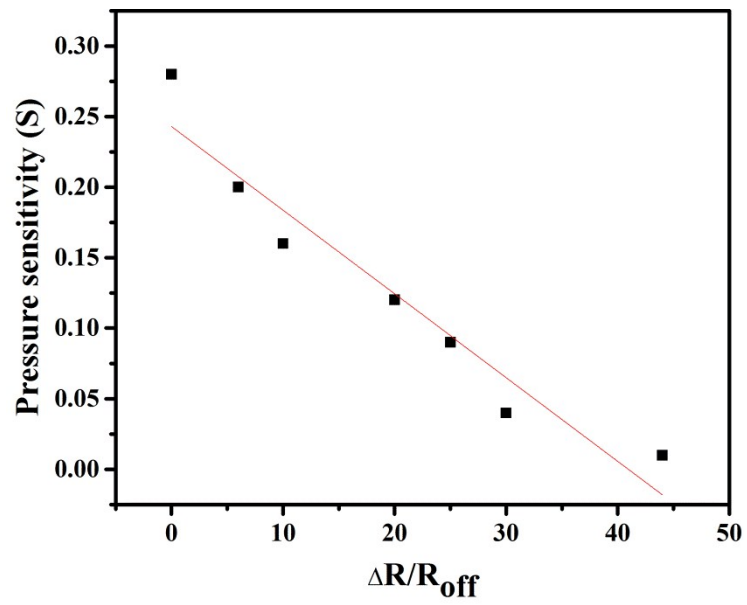


Fig. S11 The first derivative relation between pressure sensitivity S and the relative resistance $\Delta R/R_{\text{off}}$.

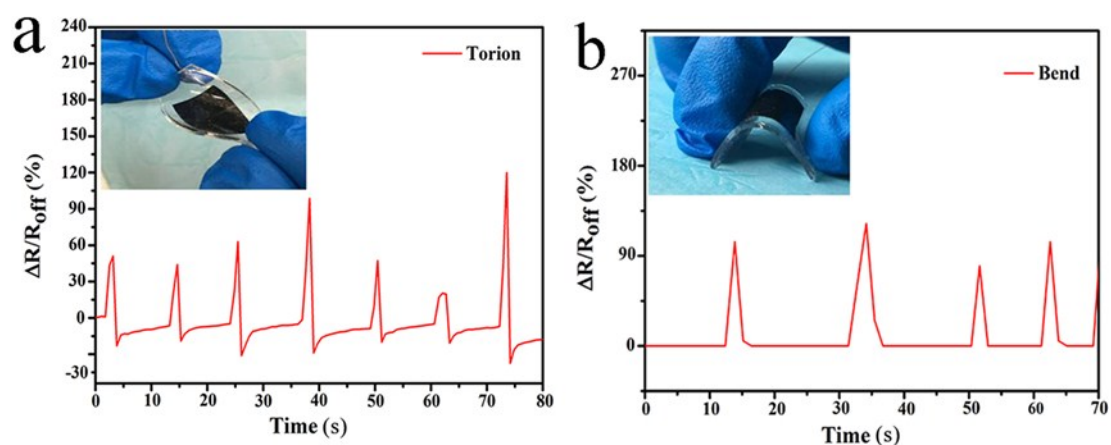


Fig. S12 Plots show the relative resistance changes to dynamic loading and unloading cycles: the deformations of (a) torsion and (b) bend. The insets are the photographs of the device under corresponding mechanical forces.

References

1. B. Qiu, M. Xing, and J. Zhang, *J. Am. Chem. Soc.* 2014, **136**, 5852–5855.
2. F. Wu, A. Xie, M. Sun, Y. Wang and M. Wang, *J. Mater. Chem. A*, 2015, **3**, 14358–14369.
3. G. Zeng, N. Shi, M. Hess, X. Chen, W. Cheng and T. Fan, *ACS. Nano*. 2015, **9**, 4227–4235.
4. H. Ha, K. Shanmuganathan and C. J. Ellison, *ACS Appl. Mater. Interfaces*. 2015, **7**, 6220–6229.